Journal of Environmental Chemical Engineering 14 (2026) 123373

Contents lists available at ScienceDirect

Journal of Environmental Chemical Engineering

journal homepage: www.elsevier.com/locate/jece

Bifunctional TiO_2 (anatase, brookite, rutile)-based photocatalysis for environment remediation: Efficient simultaneous glyphosate degradation and H_2 production

Muhammad Umair [a], Leonardo Palmisano [a], Hebah S. Jarusheh [b], Marianna Bellardita [a,*]

[a] Engineering Department, University of Palermo, Viale delle Scienze Ed. 6, Palermo 90128, Italy
[b] Department of Chemical and Petroleum Engineering, Research and Innovation Center on CO2 and Hydrogen (RICH), Khalifa University of Science and Technology, Abu Dhabi, United Arab Emirates

ARTICLE INFO

Keywords:
Wastewater treatment
Environment remediation
Glyphosate removal
Glyphosate photoreforming
Green H_2 production
Brookite TiO_2

ABSTRACT

Glyphosate is currently the most widely used herbicide in the world due to its broad-spectrum effectiveness and relatively low cost. However, its massive and prolonged application has raised serious environmental concerns. In this context, novel strategies for the effective degradation of glyphosate and its derivatives are urgently needed. One promising and sustainable approach is the use of the photocatalytic method. In this study, we explore a polyfunctional photocatalytic system capable of producing high-value compounds by oxidation of glyphosate and simultaneously obtaining H_2, a clean energy carrier. Namely, both organic and inorganic valuable compounds have been obtained by the partial oxidation of glyphosate. The effectiveness of various TiO_2-based commercial and home-prepared polycrystalline photocatalysts has been explored. Pt-TiO_2 and Cu_2O-TiO_2 heterostructured samples have been also investigated. The photocatalysts showed stability over repeated cycles and maintained their activity, indicating their practical potential. Mechanistic studies suggest that photogenerated holes were primarily responsible for the oxidative degradation of glyphosate, while photoexcited electrons drove the reduction of protons to H_2 gas. Pt-Brookite, used for the first time in this reaction, resulted in the most active photocatalyst affording about 51% of glyphosate conversion and an H_2 production of 0.34 mM.

1. Introduction

Water pollution is one of the major global challenges that human society is facing nowadays. Worldwide, around 2.1 billion people lack access to safe water, which causes millions of deaths every year [1]. The excessive use of herbicides to increase agricultural production has led to the contamination of water, generating serious environmental damage [2,3]. Glyphosate (N-phosphonomethyl glycine or PMG) is a highly effective broad-spectrum herbicide for weed control, first introduced in 1974 and marketed as Roundup [4]. The use of PMG has increased exponentially over time because it effectively and indiscriminately eradicates weeds, and genetically modified crops resistant to PMG are widely planted with the assumption that the side effects of PMG are negligible [5,6]. However, on the other hand, its massive use has caused concerns about environmental pollution because only a very small amount of applied PMG is absorbed by crops while its key intermediates, such as its metabolite aminomethylphosphonic acid (AMPA), end up in the environment [7–10]. Biologically, PMG can be degraded in soil by enzymes that act through two main processes. Through the primary degradation pathway that occurs naturally, PMG oxidoreductase cleaves the C-N bond, producing glyoxylate and AMPA [11], that is of no greater toxicological concern than its parent compound [12] although some authors report that it can have potential genotoxicity. Yue et al. [13] investigated the photodegradation of glyphosate using Bi_2WO_6 samples enriched in oxygen vacancies. The photocatalysts exhibited high removal efficiency, and toxicity-assessment tests showed that the generated intermediates were less toxic, while the final products were non-toxic. In accordance, Kuang et al. [14] carried out a toxicology evaluation on glyphosate and its intermediates after photocatalytic treatment in the presence of BiOCl nanosheets. Risk assessment of the produced intermediates was estimated by the ECOSAR program using fish, daphnia, and green algae as representative species for all aquatic organisms. They observed that glyphosate and its main degradation intermediate, AMPA, exhibit no toxicity to the three aforementioned

* Corresponding author.
E-mail address: marianna.bellardita@unipa.it (M. Bellardita).

https://doi.org/10.1016/j.jece.2026.123373
Received 27 February 2026; Received in revised form 21 May 2026; Accepted 28 May 2026
Available online 29 May 2026

organisms and are ultimately mineralized into CO_2 and H_2O.

In the second pathway, which occurs under isolated conditions, PMG C-P lyase catalyzes the cleavage of the C-P bond, forming phosphate and sarcosine [15]. The C-P lyase pathway is preferable because it produces environmentally safe products. For example, sarcosine can be further broken down into glycine and used as growth food by soil microorganisms [16]. The International Agency for Research on Cancer (IARC) has classified PMG as "Category 2a", indicating that this compound is probably carcinogenic to humans [17]. Therefore, there is a need to develop simple, effective, and environmentally friendly methods to degrade PMG into small, non-toxic inorganic molecules.

Heterogeneous photocatalysis has attracted considerable attention as a green and potentially cost-effective technology for wastewater remediation (although there is a lack of practical large-scale applications in this field) [18,19], production of high added value compounds [20] and of H_2 [21,22]. Charge separation occurs when a semiconductor is irradiated with light energy equal to or greater than its band gap energy. The degradation of pollutants in water occurs under aerobic conditions, i.e. in the presence of O_2 with the contribution of photogenerated holes that produce reactive species such as hydroxyl ($^{\bullet}OH$), superoxide ($O_2^{\bullet-}$), and hydroperoxide ($HO_2^{\bullet}$) radicals. These latter species can lead to the complete mineralization of the organic pollutants present and/or to their partial oxidation into valuable compounds [18,23]. On the other hand, photogenerated electrons can enable the formation of H_2 by water splitting or photoreforming in the presence of sacrificial agents (used to minimize the recombination of photoproduced charges) that capture the holes and partially oxidize to form high-value chemicals [24,25]. The simultaneous degradation of pollutants with H_2 production is like killing two birds with one stone: cleaning up the environment and powering the future by producing clean energy. Few studies have focused on the photocatalytic degradation of PMG [26] and only one, to the best of our knowledge, has investigated its photoreforming [27], identifying the main intermediates without providing their quantitative determination [13,14], whilst, generally, only the conversion of PMG has been evaluated [28,29]. Bamiduro et al. [30] carried out the glyphosate conversion under a 300 W xenon lamp (100 mW cm^{-2} irradiation power) and indirectly evaluated its mineralization by measuring the concentration of phosphate produced under irradiation.

TiO_2 is an n-type photocatalyst that is widely used due to its properties such as abundance, non-toxicity, high (photo)stability, high oxidizing power and relative cheapness [31]. This solid exists in various polymorphic crystalline phases, the most important of which are anatase, brookite and rutile. Its physicochemical properties and different photocatalytic activity depend on the type of phase (or mixture of phases) under investigation [24]. Anatase is generally the most active polymorph for total oxidation reactions, rutile shows some efficiency in particular reactions, brookite showed good performance for H_2 production by photoreforming of organics [21,24,32–34].

However, bare TiO_2 displays low or negligible activity towards H_2 production due to its fast recombination rate of electron and hole pairs, wide band gap (3.2 eV) and conduction band edge potential near that of H^+/H_2 reduction. Studies have shown that n-type TiO_2 samples coupled with p-type materials form an effective heterojunction, suitable for enhancing charge separation and sunlight absorption, thus increasing photoactivity [35].

For example, Cu_2O is a low cost, non-toxic and easily prepared, p-type semiconductor with a band gap of 2.2 eV and a conduction band potential more negative than that of the H^+/H_2O pair [36]. The combination of Cu_2O with TiO_2 forms a p-n heterojunction that leads to absorption in the visible region and improves the separation of photogenerated charge carriers [37–39]. Platinum (Pt), on the other hand, acts as a co-catalyst attracting the photogenerated electrons thanks to its high work function and capability to extend light absorption towards the visible light region [40,41].

In this study, we investigated the photoreforming of PMG, i.e., its degradation accompanied by the formation of high-value compounds such as formic and glycolic acids, simultaneously with H_2 production. Pt- or Cu_2O were used as co-catalysts to enhance the performance of TiO_2 based photocatalysts.

Notably, for the first time, to our knowledge, brookite TiO_2 was used for this kind of reaction in addition to other solids consisting of different TiO_2 polymorphs. Some photocatalysts, like the commercial TiO_2 P25, were used only for the sake of comparison as they are known to be particularly photoactive. Inorganic ions such as phosphate and ammonium were also obtained, confirming the degradation of PMG into harmless compounds.

Furthermore, with the aim of replacing the noble metal with less expensive non-metallic species, a 3%Cu_2O-TiO_2 heterostructure was employed as the photocatalyst, as this material had previously exhibited outstanding performance in photocatalytic H_2 production [42].

2. Experimental

2.1. Chemicals

Titanium dioxide (TiO_2, P25 Aeroxide), Platinum chloride ($PtCl_4$, BDH chemicals), ethanol (C_3H_5OH, Sigma-Aldrich), hydrochloric acid (HCl, Sigma-Aldrich), titanium tetrachloride ($TiCl_4$, Sigma-Aldrich) copper(I) oxide (Cu_2O, Riedel-de Haën) were used as received without purification. The commercial herbicide Karda (registered in the R.O.P.F. (Registro Oficial de Productos Fitosanitarios) under Nº 21.491) has been used as a source of glyphosate. It consists of a mixture containing prevalently glyphosate and amines, coco alkyl ethoxylated, alcohols (C8–22) ethoxylated, as surfactants and adjuvants.

2.2. Samples preparation

2.2.1. Anatase

Anatase was synthesized by adding $TiOSO_4$ (40 g) to distilled water (180 mL) and stirring for 2 h until a clear suspension was formed. The resulting mixture was transferred to a Pyrex bottle and heated in an oven at 100℃ for 48 h. After separating the solid formed by filtration, the latter was washed with double-distilled water to remove the sulfate ions, dried at 60 °C and finally calcined for 3 h at 600 °C.

2.2.2. Brookite

The sample TiO_2 brookite was synthesized by hydrothermal hydrolysis. Typically, distilled water (420 mL), HCl (160 mL), $TiCl_4$ (10 mL) were added to a 1 L beaker and stirred for 2 h. Then, the resulting mixture was transferred to a Pyrex bottle and heated at 100 ℃ for 48 h in an oven. The obtained powder was a mixture of brookite and rutile. The brookite was separated in the supernatant by peptizing with water at different times from the rutile (not used in this work) that was present in the precipitate.

2.2.3. Rutile

The sample rutile was prepared by adding $TiCl_4$ (20 mL) to distilled water (100 mL) and stirring for 2 h at room temperature. The resulting mixture was transferred to a Pyrex bottle and heated at 100 ℃ for 48 h in an oven. The rutile powder was obtained after drying in a rotary evaporator at 50 ℃.

2.2.4. Cu_2O-TiO_2 samples

Two different composites were obtained by mixing Cu_2O with TiO_2 P25 or Brookite in a zirconium oxide coated steel jar containing six zirconium oxide balls by using a Retsch Ball Mills, type PM100 milling. The samples were prepared according to previously determined best conditions such as 150 rpm for 2 h and 3%Cu_2O.

2.2.5. Pt loaded samples

TiO_2 P25 was modified with 0.5 wt% Pt by the photodeposition

method. Typically, distilled water (400 mL), ethanol (100 mL), $PtCl_4$ (10 mL), and the TiO_2 sample (2 g) were added to the photoreactor. Initially, the mixture was stirred for 30 min in dark with He bubbling to eliminate O_2 and then the lamp was turned on under stirring for 7–8 h. After that, mixture was filtered, washed and then dried in an oven for 5–6 h.

2.3. Characterizations

X-ray diffraction (XRD) patterns of the used samples were acquired by means of a Philips diffractometer (working at current of 30 mA and voltage of 40 kV) using CuKα radiation. The Raman spectra of the tested samples were analyzed by a BWTek-i-micro Raman Plus system connected with a 785 nm diode laser. A Flow Sorb 2300 instrument (Micromeritics) was used to calculate specific surface area (SSA) using the single-point BET technique. A Shimadzu UV−2401 PC spectrophotometer was used to acquire UV–Vis diffuse reflectance spectra (DRS) in the wavelength range 200–800 nm at room temperature using barium sulphate ($BaSO_4$) as a reference material. The band gap values of the used samples were calculated by plotting the modified Kubelka-Munk function $[F(R'_\infty)hv]^{½}$ versus the energy of the exciting light. A Perkin Elmer LS55 fluorescence spectrometer was used to record the photoluminescence (PL) spectra of the different materials in the 300–600 nm range, with a 300 nm excitation wavelength. A Nova NanoSEM (Scanning Electron Microscopy) equipment was used to examine the morphology of the tested samples. A small quantity of powder samples was put on carbon tape that was fastened to a stub made of stainless steel. STEM (Scanning Transmission Electron Microscopy) analysis has been carried out by a Thermo Scientific Talos F200i TEM 20–200 kV microscope. The samples were prepared by suspending the synthesized photocatalyst in ultra-pure water, treating the suspension with ultrasounds for 60 mins, and finally dip-coating a 300-mesh Au grid with the suspension two consecutive times. The solvent was then evaporated at room temperature. X-ray photoelectron spectroscopy (XPS) was performed using a Thermo Fisher Scientific (TFS) Escalab Xi + XPS with an AlKα X-ray 52 source. Before the XPS measurements, the samples were etched in situ with an Ar beam to remove contaminants from the top layer. For the identification of the hydroxyl radical, electron paramagnetic resonance (EPR) was performed on an EMX-nano spectrometer (Bruker Biospin Crop., Karlsruhe, Germany). A solution was prepared by mixing 100 μL of 90 μM DMPO, 100 μL of 0.5 mM catalyst (in ultrapure deionized water), and 100 μL of 1 mM H_2O_2 at room temperature. This mixture was sealed in a capillary tube with Critoseal, positioned in the sample holder, and placed in the EPR resonator. EPR parameters were set as follows: Center Field at 3480 G, Sweep Width of 100 G, modulation amplitude at 1 G, attenuation at 25 dB, and receiver gain at 40 dB. The scan was performed once with a modulation frequency of 100 kHz. A Ushio 100 W Short Arc Mercury lamp (USH102DH) served as the light source for EPR spectra acquisition under irradiation.

2.4. Photocatalytic activity

The experiments were carried out at room temperature and pressure under anaerobic conditions at natural pH in a cylindrical reactor filled with 150 mL solution. The reactor temperature was maintained at ca. 30 °C using a Pyrex cooling jacket with water circulation. The initial concentration of PMG was 1 mM and the duration of the experiments was 5 h. Initially, the reactor was filled with PMG solution and catalyst, stirred in dark for 30 min with He bubbling to achieve adsorption-desorption equilibrium and to remove the dissolved air. Then, the reaction mixture was illuminated with a UV 125 W medium pressure Hg lamp (main emission peak at 365 nm, see Figure S1) and every 30 min samples were withdrawn. The radiant power emitted by the lamp, measured by a Delta Ohm DO9721 radiometer, was 10 mW cm^{-2}. The liquid samples were filtered by using 2 μm membranes (HA, Millipore) and analyzed in a Thermo Scientific Dionex ultimate 3000 HPLC, equipped with refractive index detectors and a Diode Array. The column used was a Phenomenex REZEK ROA H^+ Organic acid, the eluent 2.5 mM H_2SO_4 aqueous solution and the flow rate 0.6 mL/min. For the determination of gaseous species (H_2 and CO_2), a gas-tight syringe of 500 μL was used and analyzed in a HP 6890 Series GC System equipped with a Supelco packed column GC 60/80 Carboxen$^{TM-1000}$ and a thermal conductivity detector (TCD). Cycling experiments were conducted by recovering and reusing the most active photocatalyst three times. Cycling experiments were carried out by recovering and reusing the most active photocatalyst three times. To identify the main active species involved in the photocatalytic degradation of PMG, runs after adding selected scavengers were carried out in the presence of the most performant photocatalyst. Namely, tert-butanol, $AgNO_3$, $Na_2C_2O_4$ were used as $^{\bullet}OH$, electrons, and holes scavengers, respectively. The cationic and anionic species deriving from glyphosate scission were analyzed using a Dionex ICS−1000 and ICS−1100 ion chromatograph equipped with IONPAC® AS23 and IONPAC® CS16 anion-exchange and cation-exchange columns, respectively. For the cation-exchange column, the mobile phase consisted of a 0.03 mol/L CH_3SO_3H solution, while for the anion-exchange column, it consisted of a mixture of 0.8 mmol/L $NaHCO_3$ and 45 mmol/L Na_2CO_3.

3. Results and discussions

Fig. 1 shows the XRD patterns of the different samples. The three phases (anatase, brookite and rutile) of TiO_2 are present in the used photocatalysts identified by the characteristic peaks at 2θ = 25.5°, 38.0°, 48.0°, 54.5° for anatase, 2θ = 25.34°, 25.69०, 30.81° for brookite and 2θ = 27.5°, 36.5°, 41°, 54.1° 56.5° for rutile. Anatase and rutile polymorphs coexist in commercial P25, while the pure phases are present in the home-prepared anatase, brookite, and rutile samples. The presence of Pt was not observed due to its low amount and high degree of dispersion on the surface of TiO_2. The 3%Cu_2O-P25 sample, in addition to the characteristic anatase and rutile peaks, presents a small peak at 2θ = 36.2°, confirming the presence of Cu_2O in the TiO_2 matrix. Compared to samples such as Pt-Brookite, 3%Cu_2O-Brookite and Pt-Rutile, the peaks of the P25 and anatase-based samples are narrower and more intense, suggesting a larger crystallite size and higher crystallinity (Table 1), which can be explained by considering their preparation at a higher temperature.

To further study the structure of the samples used, Raman spectra were recorded (Fig. 1 (B)). The bands indicated the presence of anatase phase characterized by the main peaks at 144 cm^{-1}, 197 cm^{-1}, 396 cm^{-1}, 514 cm^{-1}, and 637 cm^{-1}, brookite at 126 cm^{-1}, 152 cm^{-1}, 212 cm^{-1}, 247 cm^{-1}, 322 cm^{-1}, 364 cm^{-1}, 409 cm^{-1}, 456 cm^{-1}, 498 cm^{-1}, 543 cm^{-1}, 582 cm^{-1} and 632 cm^{-1} and rutile at 446 cm^{-1} and 613 cm^{-1} [43]. No peaks of foreign species such as Pt or Cu_2O were observed, probably due to low amounts and high degrees of dispersion on the surface of TiO_2. However, the enlargement of the anatase main peak at ca. 144 cm^{-1} in the spectra of P25 and 3%Cu_2O-P25 (Figure S3), reveals a shift towards higher wavenumber in the composite sample that can be attributed to oxygen vacancies formation [44] after the coupling with Cu_2O.

P25 showed a SSA of 52 m^2 g^{-1}, which was almost unchanged after the addition of Pt or Cu_2O. Pt-Brookite, 3%Cu_2O-Brookite and Pt-Rutile showed SSA values of 98, 91 and 85 m^2 g^{-1}, respectively. Fig. 2 (Left-side) illustrates the UV-Vis DRS spectra of the different samples. All of them are active in the UV-Vis region. P25 shows a transition edge at 360 nm, corresponding to the band gap of anatase that is mainly present, while rutile is in a lower amount. The colour of the samples turned grayish after the addition of platinum and pink after coupling with Cu_2O, and consequently, a decrease in reflectance was observed in these powders. Pt-Rutile showed the lowest band gap value (3.02 eV), and its transition edge shifted towards higher wavelength, while Brookite displayed the highest figure, in accordance with literature [32] .

PL spectra can be used to determine the tendency of photocatalysts to

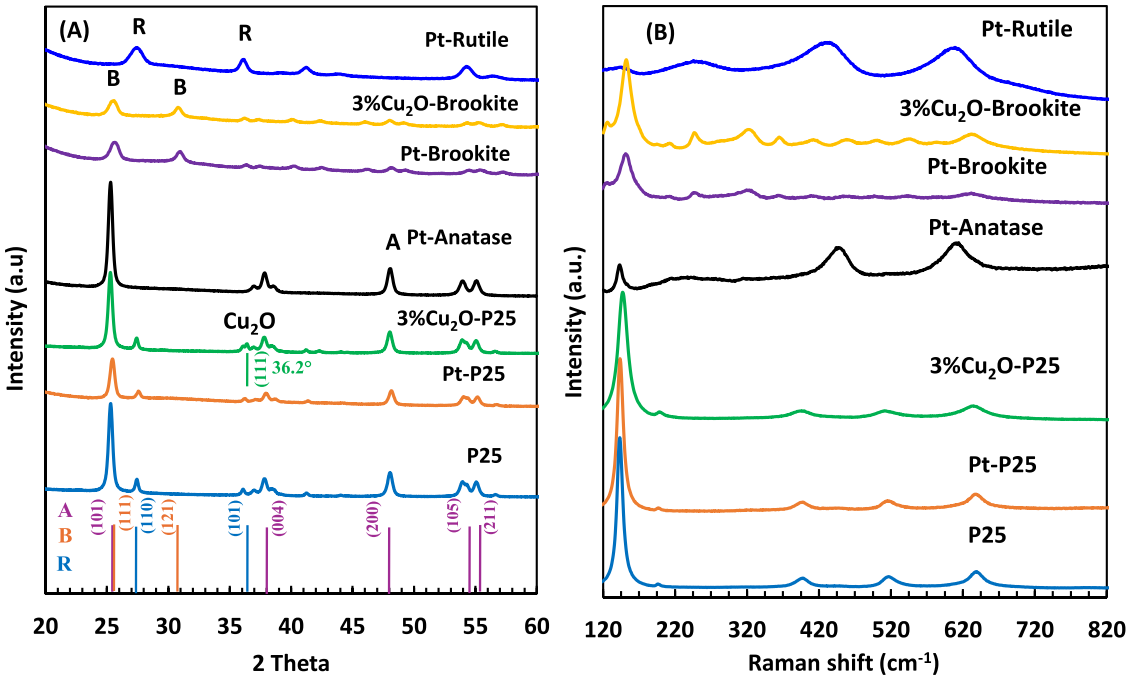

Fig. 1. (A) XRD patterns and (B) Raman spectra of different samples used.

Table 1
TiO_2 phase (A=Anatase, R=Rutile, B= Brookite), specific surface area (SSA) and band-gap (Eg) for the different samples.

Sample	Crystalline phase	SSA ($m^2 \cdot g^{-1}$)	E_g (eV)
P25	A, R	52	3.18
Pt-P25	A, R	50	3.10
Pt-Anatase	A	50	3.26
Pt-Brookite	B	98	3.34
Pt-Rutile	R	85	3.02
3%Cu_2O-P25	A, R	48	3.08
3%Cu_2O-Brookite	B	91	3.32

charge transfer and recombination of photogenerated pairs. A high PL emission intensity indicates a fast rate of electron-hole recombination, which is detrimental to photocatalytic efficiency because it means that fewer charge carriers are available for the desired reaction. Fig. 2 (right side) reports the PL spectra of the various photocatalysts. All samples show peaks at around 420, 475 and 530 nm, and the addition of foreign species did not change the shape of the spectra, indicating that they do not give rise to new radiative phenomena but only to an increase in the transfer rate of the photogenerated charges, as the intensity is reduced. The main band at approximately 420 nm originates from the transition of promoted electrons from the conduction band back to the valence band in TiO_2, and it is consistent with the band gap values. The bands at longer wavelengths can instead be attributed to the non-radiative recombination of electrons in some lattice defects [45]. The addition of Pt or Cu_2O caused a decrease in the band intensity, indicating a less significant recombination of the photogenerated electron-hole pairs, and suggesting the occurrence of an increase in photocatalytic performance compared to the corresponding bare samples.

SEM images were acquired (Fig. 3) to study the morphology of the different photocatalysts. All powders showed the presence of aggregates of irregularly shaped particles, whose dimensions ranged from 30 to

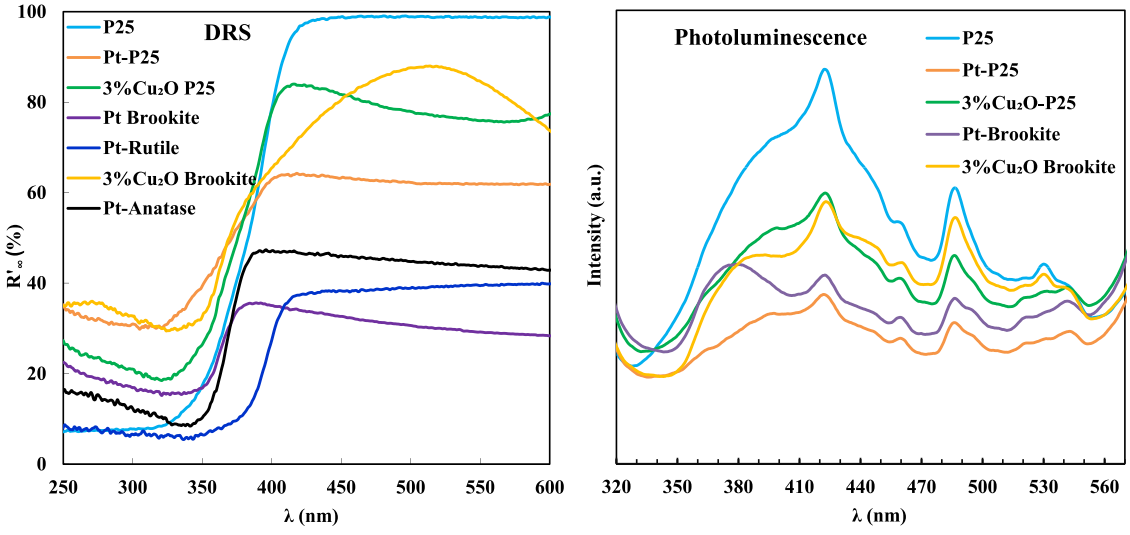

Fig. 2. UV-Vis DRS and PL spectra of different samples used.

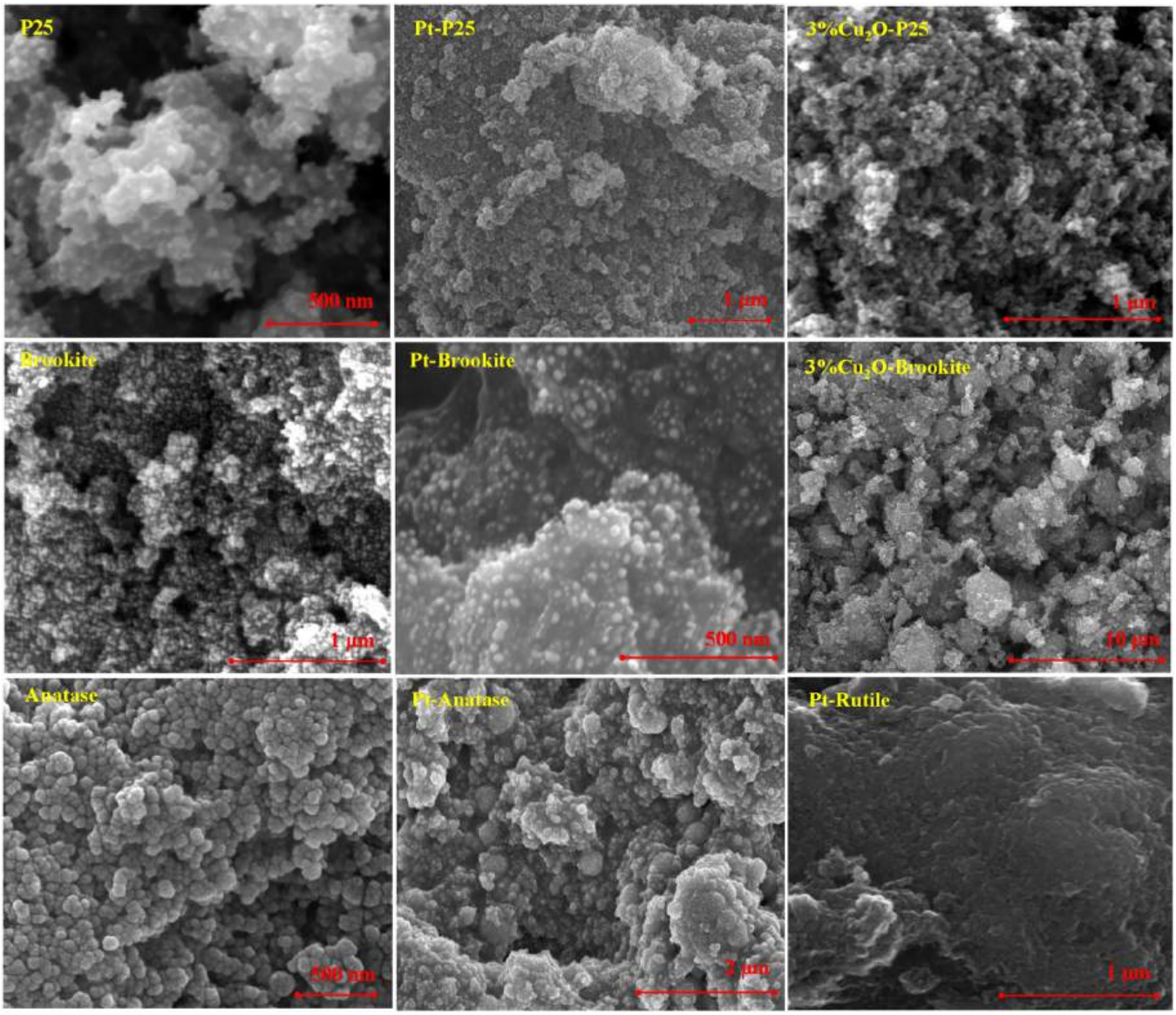

Fig. 3. SEM images of different samples used.

140 nm. The presence of foreign species (Pt or Cu_2O) was not observed, likely due to their low loading and homogeneous dispersion within the TiO_2 framework. As a result, the overall morphology closely resembled that of the bare TiO_2 samples. Therefore, the different photoactivities

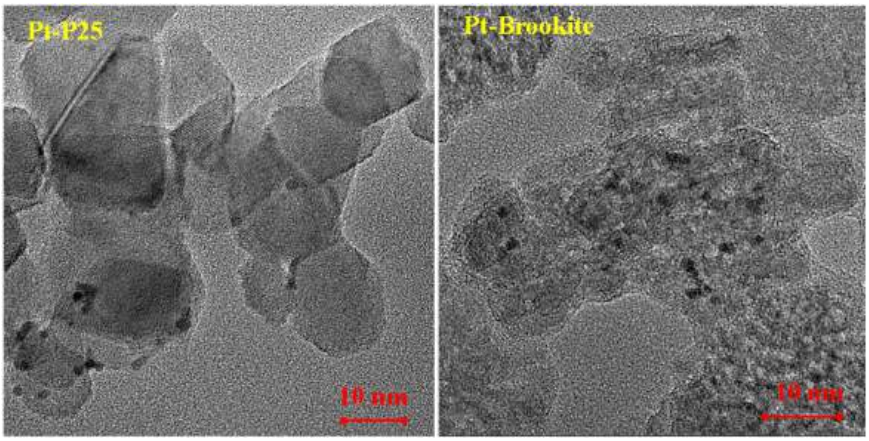

Fig. 4. TEM images of Pt-P25 and Pt-Brookite photocatalysts.

observed (see Section 4) cannot be attributed to variations in sample morphology.

Fig. 4 shows TEM images of the Pt–TiO_2 powders. An island distribution of Pt nanoparticles on the TiO_2 surface can be observed. The Pt particle size is similar in both photocatalysts, with an average diameter of approximately 2–3 nm. Therefore, it is reasonable to assume that the differences in photocatalytic performance observed among the samples are not attributable to variations in Pt particle size.

STEM-EDS mapping of the Pt-Brookite and 3%Cu_2O-P25 samples confirmed the presence of Ti, O, Pt, and Cu species (Fig. 5). In the Pt-Brookite sample, Pt atoms appear non-uniformly dispersed, a behaviour attributable to the photodeposition method and the low Pt loading (0.5 wt%), which results in only trace amounts being detectable. Conversely, in the 3%Cu_2O-P25 composite, Cu_2O is homogeneously distributed across the P25 surface. This is in accordance with the preparation method being the two commercial oxides combined via ball milling, and with the Cu_2O loading being higher at 3 wt%.

The XPS Ti 2p core-level spectrum of TiO_2 exhibits a characteristic spin-orbit doublet consisting of Ti $2p_{3/2}$ and Ti $2p_{1/2}$ components at 459.5 eV and 465.0 eV, respectively [46]. Fig. 6 confirmed that in TiO_2 P25, titanium is predominantly in the Ti^{4+} oxidation state and revealed that the addition of Cu_2O induced a partial reduction of Ti^{4+} to Ti^{3+}. XPS analysis of the Ti 2p region in Pt-Brookite showed that the addition of platinum also resulted in a partial reduction of Ti^{4+} to Ti^{3+}. The appearance of a Ti^{3+} component at a lower binding energy (ca. 457–458 eV) in the Ti $2p_{3/2}$ spectrum confirms the electronic interaction between the foreign materials (Cu_2O or Pt) and the TiO_2 support [47]. The O 1 s spectrum was deconvoluted into three peaks. The peak centered at approximately 530 eV (O_L) corresponds to lattice oxygen in metal-oxygen bonds (Ti-O) [48]. The peak at a higher binding energy of approximately 532 eV is assigned to non-lattice oxygen species, including surface-adsorbed oxygen and hydroxyl groups introduced during sample handling [48]. The peak centered at approximately 534 eV is attributed to O-C bonds. Upon the addition of Cu_2O, an additional peak appeared at a lower binding energy of approximately 529 eV, which is associated with lattice oxygen in Cu-O bonds [49]. The Cu 2p spectrum revealed different components. The main peaks at approximately 932.8 eV and 952.8 eV can be assigned to Cu^+ [36,50,51]. A secondary feature at around 941.2 eV corresponds to the Cu^{2+} $2p_{3/2}$ satellite transition [50,52]. This spectral pattern indicates the presence of only a minor fraction of Cu^+, consistent with the limited stability of Cu oxidation states under the investigated conditions.

XPS spectra confirmed the presence of platinum on Brookite, with a signal observed at approximately 71 eV. The high-resolution Pt 4 f spectrum corresponds to the Pt $4f_{5/2}$ and Pt $4f_{7/2}$ spin-orbit components. However, due to the low Pt loading on the sample, only a weak signal was detected, making it difficult to determine the oxidation state of platinum.

EPR spectra of P25, 3%Cu_2O-P25 and Pt-Brookite samples were acquired in both the absence and presence of illumination (for 15 min), as highlighted in Fig. 7. Experiments conducted in the absence of light fail to detect any EPR signal, indicating that DMPO has little to no paramagnetic center and that the photocatalysts are incapable of producing radicals in the dark. Upon opening the shutter and illuminating the suspension containing the photocatalysts, their EPR spectra show the characteristic four-peak paramagnetic resonance pattern of hydroxyl radicals ($^{\bullet}OH$), a distinctive feature of the DMPO-$^{\bullet}OH$ adduct, with varying signal intensities. These findings indicate that all tested photocatalysts are thermodynamically capable of generating hydroxyl radicals under illumination, given that their conduction band edges lie at more negative potentials than the $^{\bullet}OH/H_2O_2$ redox potential (0.87 V, NHE) [53]. These data suggest that the photocatalytic mechanism involves the generation of hydroxyl radicals. The higher intensity recorded for the modified TiO_2 samples indicates their higher capability to generate $^{\bullet}OH$ species with respect to bare P25.

4. Photocatalytic activity

All TiO_2-based samples were tested under UV irradiation in anaerobic conditions. In this study, we compared commercial P25 and different phases (Anatase, Brookite, and Rutile) of home-prepared TiO_2 based photocatalysts modified with Pt or Cu_2O. Conversion (X) and selectivity (S) towards the products were calculated by using the following Eqs. 1 and 2:

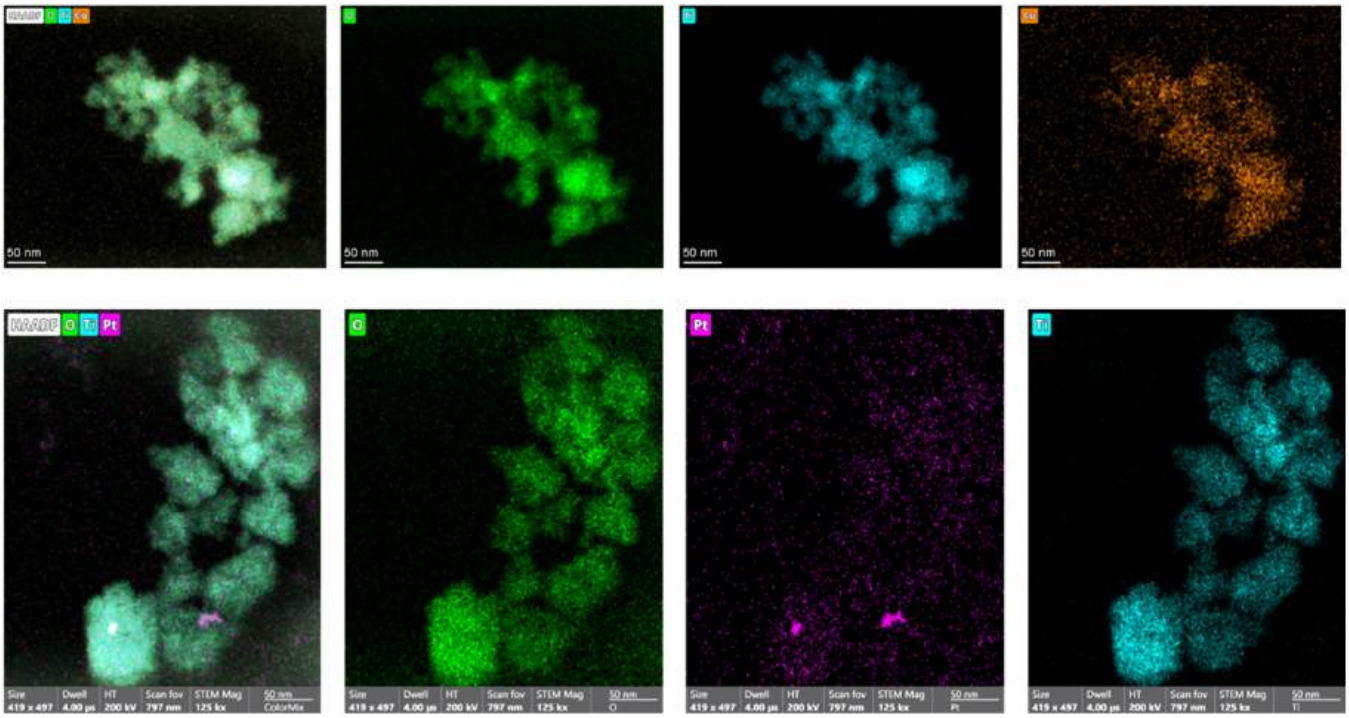

Fig. 5. STEM images of the samples: 3%Cu_2O-P25 (upper) and Pt-Brookite (lower).

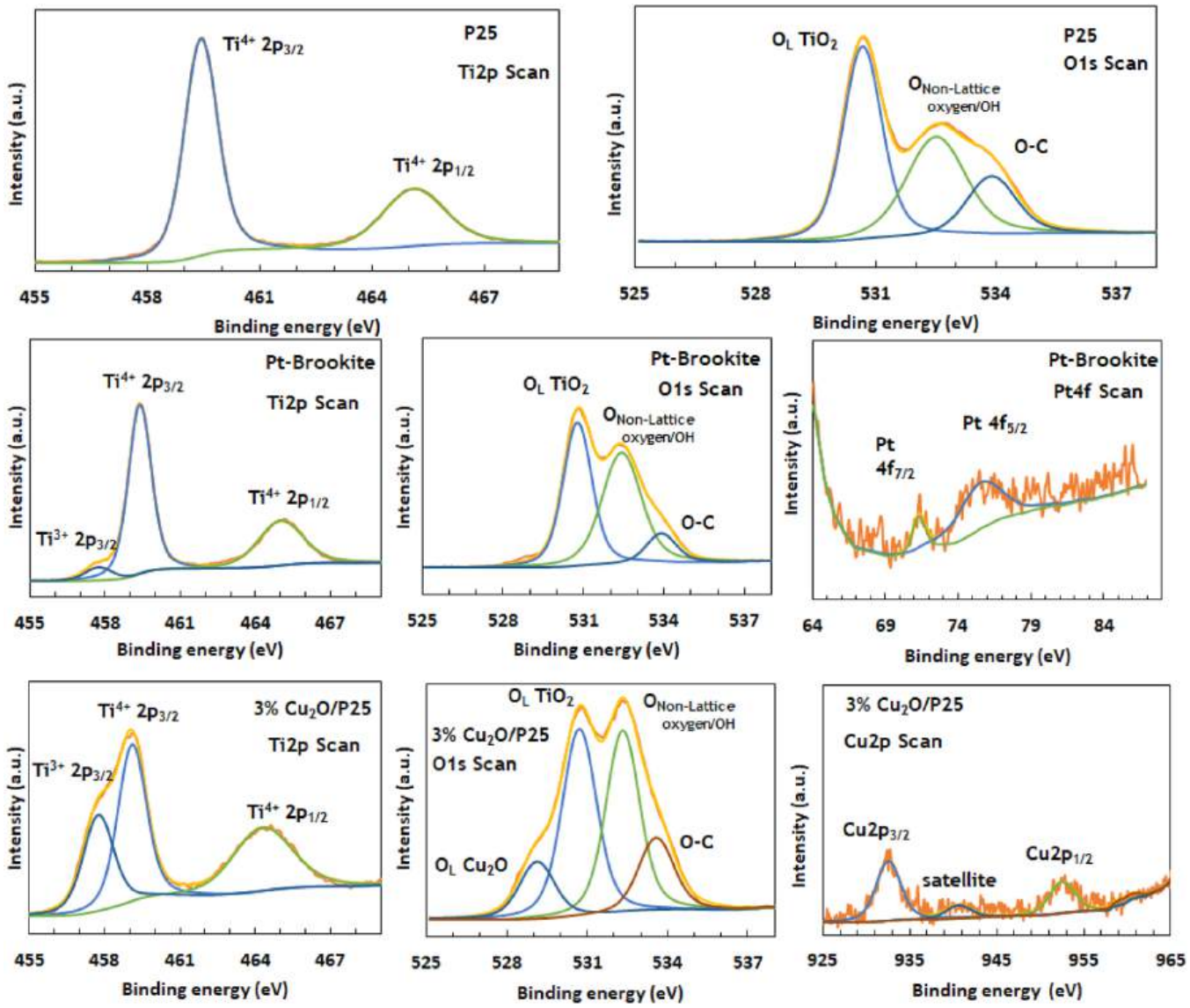

Fig. 6. XPS spectra of P25, Pt-Brookite and 3%Cu_2O-P25 catalysts.

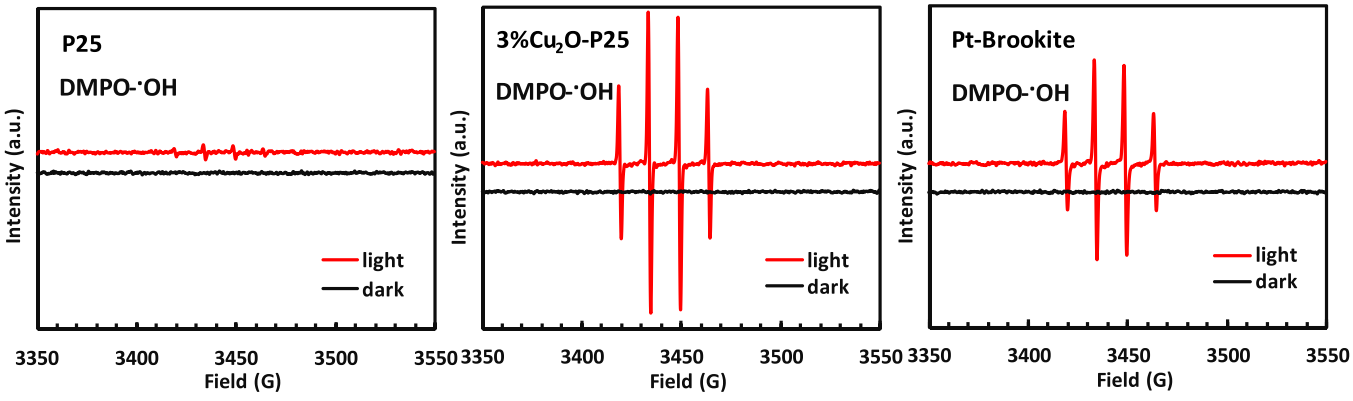

Fig. 7. EPR spectra of the DMPO-hydroxyl radicals adduct generated by the P25, 3%Cu_2O-P25 and Pt-Brookite photocatalysts under both dark and irradiation.

$$X = \left[\frac{C_i - C_t}{C_i}\right] \times 100 \quad (1)$$

$$S = \left[\frac{P_t}{C_i - C_t}\right] \times \quad 100 \quad (2)$$

where C_i represents the initial PMG molar concentration, C_t shows the

molar concentration at any time interval t and P_t is the molar concentration of the product at any time t.

Regarding the glyphosate derivatives formed during its degradation, formic acid and glyoxylic acid are the only organic intermediates present in the chromatogram. Table 2 shows the results obtained during the degradation of PMG (1 mM), comparing the conversion and the selectivity values towards the intermediate products formed in the liquid phase, i.e., formic acid and glyoxylic acid, over 5 h of irradiation. The amounts of gaseous species (H_2 and CO_2) accumulated in the headspace of the reactor are also reported. No H_2 production was observed in the presence of bare P25 due to poor charge separation and the intrinsic low energetic efficiency of this photocatalyst towards H_2 production [21, 24]. PMG conversion was 14%, along with formic acid selectivity of 83% (no glyoxylic acid was observed) and a fair degree of mineralization. Pt, due to the higher value of its work function [54,55], is recognized as the most active metallic co-catalyst for H_2 production, because, acting as an electron sink, enhances the separation of photogenerated electron-hole pairs. For this reason, Pt has been photodeposited on the different photocatalysts. In the presence of Pt-P25, conversion increased 1.78 times compared to bare P25, with selectivity reaching 100 and 35% towards formic acid and glyoxylic acid, respectively. At the same time, the amounts of H_2 and CO_2 produced were 0.11 and 0.009 mM, respectively. To replace Pt with non-metallic species, a 3%Cu_2O-P25 composite was tested, which proved to be very active for glycerol photoreforming even under direct sunlight [42]. The coupling of Cu_2O with TiO_2 demonstrated effectiveness for H_2 production even in the photoreforming of PMG, although the conversion and selectivity values were lower than those obtained in the presence of Pt-P25. However, in our opinion, these results not only confirm the efficacy of Cu_2O in replacing noble metals for H_2 production, but also suggest that its behaviour should be further investigated in the future [42].

To investigate whether the home-prepared brookite, which has proven effective for H_2 production, also exhibits activity in this reaction, Pt-loaded brookite was selected as the photocatalyst [24]. Also in this case, this photocatalyst turned out to be the best one, allowing a PMG conversion of 51% and a selectivity towards formic and glyoxylic acids of 100% and 20%, respectively (Fig. 8) with a contemporary maximum H_2 formation of 0.34 mM. The high H_2 production can be ascribed to a synergistic effect between electronic and surface brookite features. The rutile phase (Pt-rutile) showed the lowest activity for PMG conversion and no H_2 production was observed, probably due to the higher recombination of the photoproduced pairs and thermodynamically unfavorable intrinsic electronic properties.

Pt-anatase was more active than Pt-rutile due to the more negative conduction band position of anatase compared to rutile [56], giving a PMG conversion of 28% with H_2 production of 0.15 mM and selectivity values of 73 and 19% towards formic and glyoxylic acid, respectively. Brookite, the least common TiO_2 polymorph, exhibits peculiar features as a higher redox potential than anatase and rutile [57], higher hydroxylation degree [58] and higher ability to adsorb water [24].

Table 2
Results obtained during glyphosate photoreforming (1 mM) after 5 h of UV irradiation using a 125 W medium pressure Hg lamp under anaerobic conditions. X = Conversion; S= Selectivity.

Sample	$X_{Glyphosate}$ (%)	$S_{Formic\ acid}$ (%)	$S_{Glyoxylic\ acid}$ (%)	H_2 [mM]	CO_2 [mM]
P25	14	83	-	0.00	0.0062
Pt-P25	25	100	35	0.11	0.0089
3%Cu_2O-P25	19	82	18	0.14	0.0080
Pt-Brookite	51	100	20	0.34	0.0043
3%Cu_2O-Brookite	28	65	16	0.05	0.0168
Pt-Anatase	28	73	19	0.15	0.0091
Pt-Rutile	9	100	-	0.00	0.0065

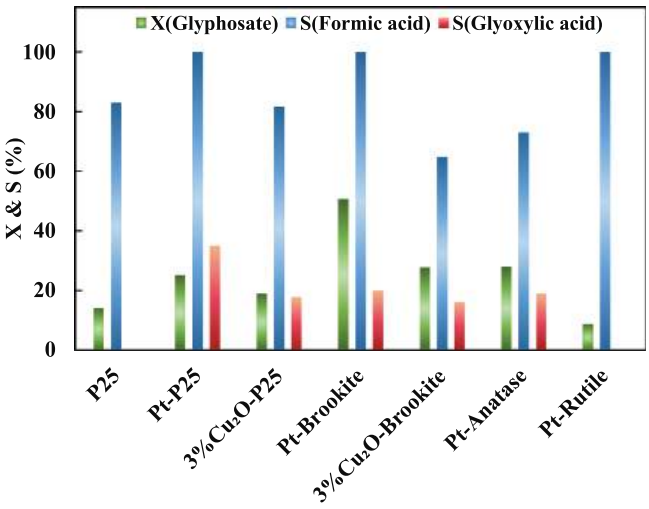

Fig. 8. Glyphosate conversion (X) and selectivity (S) towards formic acid and glyoxylic acid in the presence of the different photocatalysts after 5 h of irradiation.

Notably, although the partial oxidation of PMG has been investigated by some authors [59], no quantitative data related to the formed intermediates are reported.

In Fig. 9 are reported the results obtained during three consecutive runs carried out by using Pt-Brookite as the photocatalyst in terms of glyphosate conversion (ratio between the concentration under irradiation onver the initial one) and H_2 production. Regarding glyphosate conversion, a slight decrease in activity was observed, likely due to both the small loss of catalyst between runs and the possible permanence of small amounts of residual species adsorbed on the surface. This, however, did not substantially compromise hydrogen formation.

The effective cleavage of C–N or C–P bonds in glyphosate (Fig. 5) is indicated by the high selectivity towards formic acid, which might have been facilitated by the Pt-based catalysts (highlighted as blue in Table 2). Formic acid and glyoxylic acid are both valuable chemicals with important industrial and commercial applications. For example, formic acid is used as an intermediate in the production of formaldehyde-free resins [60,61] and as a preservative and antibacterial agent [62]. Glyoxylic acid is used as a reducing agent in the preparation of different chemicals, as an intermediate for glycine (an amino acid used in the food and pharmaceutical industries) preparation [63], in the synthesis of vanillin (used as a flavouring and fragrance chemical) [64], as a starting material for allantoin (used in the cosmetic industry) [65] and as a precursor in the production of imidazoles, oxazoles and other

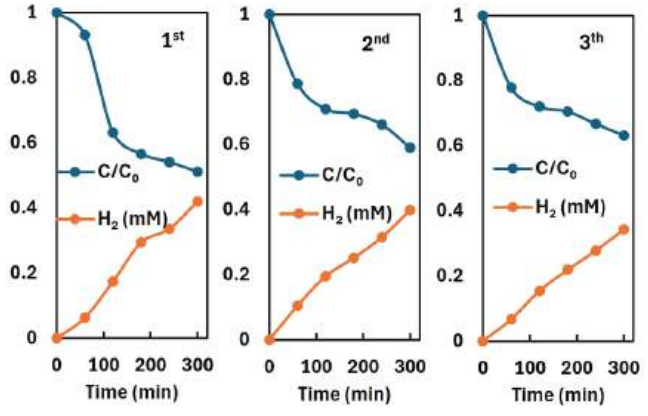

Fig. 9. Glyphosate conversion and H_2 evolution during three consecutives runs carried out in the presence of the Pt-brookite sample.

heterocycles .

A possible reaction pathway has been hypothesized in Fig. 10. PMG undergoes bond cleavage through two probable roots, leading to the formation of high-value intermediates and ultimately to mineralization with the formation of inorganic phosphate, ammonia, and CO_2.

In turn, the photoproduced electrons drive the reduction of protons to H_2. Then, the combined process allows environmental remediation, transforming glyphosate, its valorization obtaining high added value compounds by partial oxidation and the production of a renewable fuel by the electrons.

Fig. 10 schematically illustrates the hypothesized reaction pathways occurring during PMG photoreforming. Cleavage of the C-N bond can lead to the formation of glyoxylic acid, followed by further cleavage to formic acid, and finally mineralization to CO_2, H_2O. In the same time H^+ cleavage gives rise to H_2 by means of electrons. The parallel pathway involving the cleavage of the C-P and C-N bonds produces two ionic species: phosphate and ammonia. Also, these latter can be considered valuable compounds as they find application in the fertilizer industry. Moreover, the formation of phosphate and ammonia indicates that AMPA, one possible intermediate deriving from glyphosate, does not accumulate in the reaction mixture [5,13,30]. Naturally, the possibility that AMPA may form transiently in small amounts and subsequently undergo further degradation cannot be excluded.

In Table 3, phosphate and ammonium concentrations measured by ion chromatography during the photoreforming of PMG in the presence of Pt-Brookite and Pt-P25 are reported. During the photocatalytic reaction a continuous increase in concentration was determined for both species, showing a progressive cleavage of the C–P and C–N bonds present in PMG molecule. In agreement with [30], the formation of these ions provides an indirect assessment of the photocatalytic mineralization of glyphosate under irradiation. Furthermore, for the same reasons, the results also allow us to deduce that AMPA does not accumulate in the reaction medium, since the AMPA that is formed is subsequently degraded.

Table S1 compares glyphosate degradation using different semiconductor photocatalysts. Although some studies report higher levels of degradation than those obtained in this work, most studies focus exclusively on monitoring herbicide disappearance. Only few of them also evaluate total organic carbon, the evolution of intermediate species, or H_2 production.

The catalyst that proved to be the best, i.e., Pt-Brookite, was tested in the presence of different scavengers to identify the main reactive species involved in PMG degradation (Fig. 11A). After the addition of $AgNO_3$, no substantial change in PMG conversion was observed suggesting that electron trapping favours the oxidation reaction enhancing holes transfer to the substrate.

On the other hand, both the presence of tert-butanol ($^{\bullet}OH$ trap) and $Na_2C_2O_4$ (h^+ trap), competing with water, significantly reduced the degradation efficiency, indicating that hydroxyl radicals ($^{\bullet}OH$) and holes (h^+), play an important role, in accordance with Ali and Alwared [66]. The comparison of the photocatalytic activity in the experiment without scavengers, however, suggests that several reactive species synergistically participate in the overall photocatalytic activity.

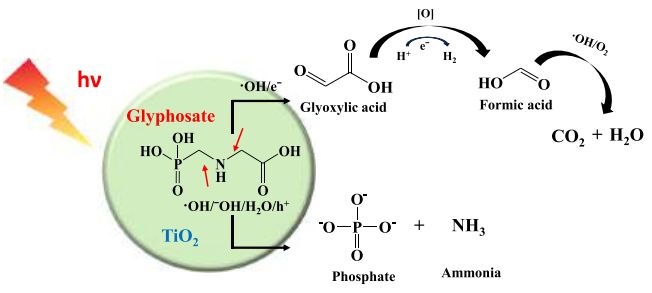

Fig. 10. Reaction scheme of glyphosate photoreforming.

Table 3
Concentrations of phosphate and ammonia in the presence of Pt-Brookite and Pt-P25.

	Pt-Brookite		Pt-P25	
	C (mM)		C (mM)	
T (min)	Phosphate	Ammonium	Phosphate	Ammonium
0	0	0	0	0
120	0.059	0.034	0.086	0.028
240	0.130	0.057	0.150	0.060
300	0.149	0.065	0.231	0.075

Monitoring the production of H_2 during irradiation (Fig. 11B) reveals three key trends. First, adding tert-butanol does not noticeably affect the amount of H_2 formed, indicating that hydroxyl radicals do not play a significant role in the H_2 production pathway. Second, introducing $Na_2C_2O_4$ leads to a slight increase in H_2 production, which can be attributed to the higher availability of electrons after holes scavenging by oxalate. Finally, when $AgNO_3$ is present, no H_2 is produced at all, consistent with the fact that silver ions efficiently scavenge electrons.

In Table 4 the ammonia and phosphate concentrations, in the absence and presence of scavengers, are compared during the irradiation time. After adding tert-butanol and $Na_2C_2O_4$ the concentration of the ionic species is lower than that observed in their absence, confirming the active role of $^{\bullet}OH$ and h^+ in PMG degradation, in accordance with the data reported in Fig. 11. Following the addition of $AgNO_3$, the ammonia concentration increases, indicating that trapping of photogenerated electrons suppress the charges recombination, thereby enhancing the oxidation reaction. Conversely, the amount of phosphate decreases with respect to the experiment in the absence of $AgNO_3$, and this result is difficult to rationalize, although a tentative explanation could be the interaction between Ag^+ and phosphate ions producing poorly soluble Ag_3PO_4.

5. Conclusion

This work investigates glyphosate photoreforming in the presence of selected TiO_2 based photocatalysts with the aim of verifying the feasibility of the process. Namely, the runs were carried out under anaerobic conditions to exploit the possibility of the contemporary oxidation/partial oxidation of PMG and H_2 production. The system successfully achieved this objective by simultaneously addressing three key aspects: (i) environmental remediation through the degradation of glyphosate; (ii) generation of value-added compounds via its partial oxidation; and (iii) concurrent H_2 production. In other words, one process delivers environmental, chemical, and energy benefits simultaneously. Notably, TiO_2 Pt-Brookite, used for the first time in this reaction, proved to be the best performing photocatalyst, confirming the effectiveness of this TiO_2 polymorph in H_2 production due to some peculiar features as strong redox potential than anatase and rutile, higher hydroxylation degree, and higher ability to adsorb water.

To the best of our knowledge, this study represents one of the first examples in which three objectives are achieved simultaneously, establishing a new paradigm in environmental remediation that integrates contaminant degradation with energy generation and chemicals production. This approach opens new opportunities for the design of multifunctional photocatalysts tailored to specific pollutants degradation/valorization. In conclusion, future developments of this preliminary work should focus on the exploration of novel photocatalysts and on the integration of suitable separation systems with the reactor to enable the efficient recovery of the value-added chemicals produced.

CRediT authorship contribution statement

Leonardo Palmisano: Writing – review & editing. **Muhammad Umair:** Writing – original draft, Investigation. **Marianna Bellardita:** Writing – review & editing, Writing – original draft, Visualization,

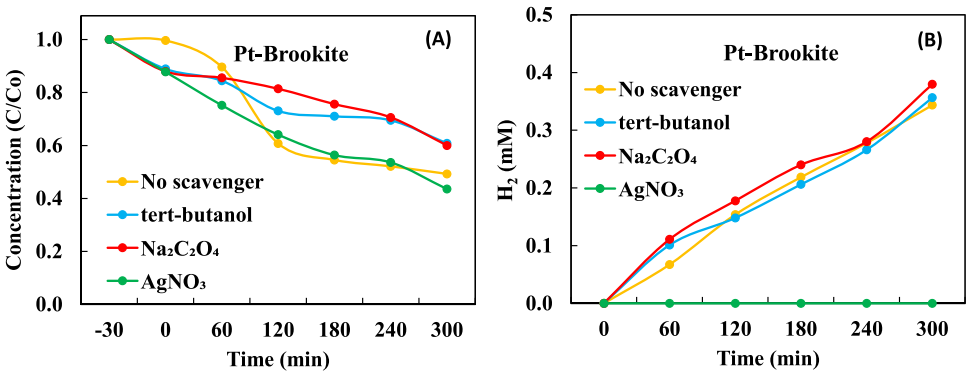

Fig. 11. Comparison of PMG degradation (A) and H_2 evolution (B) by using Pt-Brookite in the presence of different scavengers.

Table 4
Concentrations of phosphate and ammonia in the presence of Pt-Brookite and different scavengers.

	tert-butanol		$Na_2C_2O_4$		$AgNO_3$	
T (min)	**Phosphate**	**Ammonium**	**Phosphate**	**Ammonium**	**Phosphate**	**Ammonium**
−30	0	0	0	0	0	0
120	0.029	0.058	0.031	0.064	0.025	0.093
240	0.050	0.123	0.055	0.154	0.041	0.171
300	0.063	0.147	0.065	0.005	0.048	0.200

Supervision, Conceptualization. **Hebah S. Jarusheh:** Investigation.

Declaration of Competing Interest

The authors declare that they have no known competing financial interests or personal relationships that could have appeared to influence the work reported in this paper.

Acknowledgements

M.U. thanks SiciliAn MicronanOTecH Research And Innovation Center "SAMOTHRACE" (MUR, PNRR-M4C2, ECS_00000022), spoke 3 - Università degli Studi di Palermo "S2-COMMs - Micro and Nanotechnologies for Smart & Sustainable Communities" for financial support. M. B. thanks Prof. Giovanni Palmisano (Khalifa University, Abu Dhabi, UAE) for TEM, XPS, and EPR measurements.

Appendix A. Supporting information

Supplementary data associated with this article can be found in the online version at doi:10.1016/j.jece.2026.123373.

Data availability

No data was used for the research described in the article.

References

[1] N. Pichel, M. Vivar, M. Fuentes, The problem of drinking water access: A review of disinfection technologies with an emphasis on solar treatment methods, Chemosphere 218 (2019) 1014–1030, https://doi.org/10.1016/j.chemosphere.2018.11.205.
[2] A. Parven, I.M. Meftaul, K. Venkateswarlu, M. Megharaj, Herbicides in modern sustainable agriculture: environmental fate, ecological implications, and human health concerns, Int. J. Environ. Sci. Technol. 22 (2025) 1181–1202, https://doi.org/10.1007/s13762-024-05818-y.
[3] W. Zhou, M. Li, V. Achal, A comprehensive review on environmental and human health impacts of chemical pesticide usage, Emerg. Contam. 11 (2025) 100410, https://doi.org/10.1016/j.emcon.2024.100410.
[4] S.O. Duke, S.B. Powles, Glyphosate: a once-in-a-century herbicide, Pest. Manag. Sci. 64 (2008) 319–325, https://doi.org/10.1002/ps.1518.
[5] L. Cao, D. Ma, Z. Zhou, C. Xu, C. Cao, P. Zhao, Q. Huang, Efficient photocatalytic degradation of herbicide glyphosate in water by magnetically separable and recyclable BiOBr/Fe_3O_4 nanocomposites under visible light irradiation, Chem. Eng. J. 368 (2019) 212–222, https://doi.org/10.1016/j.cej.2019.02.100.
[6] R. Annett, H.R. Habibi, A. Hontela, Impact of glyphosate and glyphosate-based herbicides on the freshwater environment, J. Appl. Toxicol. 34 (2014) 458–479, https://doi.org/10.1002/jat.2997.
[7] O.K. Borggaard, A.L. Gimsing, Fate of glyphosate in soil and the possibility of leaching to ground and surface waters: a review, Pest. Manag. Sci. 64 (2008) 441–456, https://doi.org/10.1002/ps.1512.
[8] S. Singh, V. Kumar, S. Datta, A.B. Wani, D.S. Dhanjal, R. Romero, J. Singh, Glyphosate uptake, translocation, resistance emergence in crops, analytical monitoring, toxicity and degradation: a review, Environ. Chem. Lett. 18 (2020) 663–702, https://doi.org/10.1007/s10311-020-0.
[9] S. Singh, V. Kumar, J.P.K. Gill, S. Datta, S. Singh, V. Dhaka, D. Kapoor, A.B. Wani, D.S. Dhanjal, M. Kumar, et al., Herbicide glyphosate: toxicity and microbial degradation, Int. J. Environ. Res. Public. Health 17 (2020) 7519, https://doi.org/10.3390/ijerph17207519.
[10] V.C. Aparicio, E. De Gerónimo, D. Marino, J. Primost, P. Carriquiriborde, J. L. Costa, Environmental fate of glyphosate and aminomethylphosphonic acid in surface waters and soil of agricultural basins, Chemosphere 93 (2013) 1866–1873, https://doi.org/10.1016/j.chemosphere.2013.06.041.
[11] H. Zhan, Y. Feng, X. Fan, S. Chen, Recent advances in glyphosate biodegradation, Appl. Microbiol. Biotechnol. 102 (2018) 5033–5043, https://doi.org/10.1007/s00253-018-9035-0.
[12] P.K. Gupta, Herbicides and fungicides, in: R.C. Gupta (Ed.), Reproductive and Developmental Toxicology, Academic Press, 2022, pp. 665–689, https://doi.org/10.1016/B978-0-323-89773-0.00035-7.
[13] C. Yue, H. Zhou, L. Chen, H. Wang, X. Wu, Q. Yan, H. Zhang, S. Yang, Efficient visible light-driven photodegradation of glyphosate utilizing Bi_2WO_6 with oxygen vacancies: performance, mechanism, and toxicity assessment, Environ. Pollut. 348 (2024) 123876, https://doi.org/10.1016/j.envpol.2024.123876.
[14] Z. Kuang, N. Fang, X. Deng, W. Yu, S. Su, Y. Chu, Modulating the morphology and oxygen vacancies of BiOCl for efficient photocatalytic degradation of glyphosate, J. Environ. Chem. Eng. 14 (3) (2026) 122287, https://doi.org/10.1016/j.jece.2026.122287.
[15] C.A. Villamar-Ayala, J.V. Carrera-Cevallos, R. Vasquez-Medrano, P.J. Espinoza-Montero, Fate, eco-toxicological characteristics, and treatment processes applied to water polluted with glyphosate: a critical review, Crit. Rev. Environ. Sci. Technol. 49 (2019) 1476–1514, https://doi.org/10.1080/10643389.2019.1579627.
[16] Y. Huang, Z. Li, K. Yao, C. Chen, C. Deng, Y. Fang, R. Li, H. Tian, Suppressing toxic intermediates during photocatalytic degradation of glyphosate by controlling adsorption modes, Appl. Catal. B Environ. 299 (2021) 120671, https://doi.org/10.1016/j.apcatb.2021.120671.
[17] IARC Working Group on the Evaluation of Carcinogenic Risks to Humans, Some organophosphate insecticides and herbicides, International Agency for Research on Cancer, Lyon, France, 2017.
[18] U.I. Gaya, A.H. Abdullah, Heterogeneous photocatalytic degradation of organic contaminants over titanium dioxide: a review of fundamentals, progress and problems, J. Photochem. Photobiol. C Photochem. Rev. 9 (2008) 1–12, https://doi.org/10.1016/j.jphotochemrev.2007.12.003.
[19] R. Molinari, F. Pirillo, V. Loddo, L. Palmisano, Heterogeneous photocatalytic degradation of pharmaceuticals in water by using polycrystalline TiO_2 and a

nanofiltration membrane reactor, Catal. Today 118 (2006) 205–213, https://doi.org/10.1016/j.cattod.2005.11.091.
[20] G. Palmisano, V. Augugliaro, M. Pagliaro, L. Palmisano, Photocatalysis: a promising route for 21st century organic chemistry, Chem. Commun. (2007) 3425–3437, https://doi.org/10.1039/B700395C.
[21] M. Bellardita, E.I. García-López, G. Marcì, L. Palmisano, Photocatalytic formation of H₂ and value-added chemicals in aqueous glucose (Pt)-TiO₂ suspension, Int. J. Hydrog. Energy 41 (2016) 5934–5947, https://doi.org/10.1016/j.ijhydene.2016.02.103.
[22] J. Du, S. Ma, H. Liu, H. Fu, L. Li, Z. Li, Y. Li, J. Zhou, Uncovering the mechanism of novel AgInS₂ nanosheets/TiO₂ nanobelts composites for photocatalytic remediation of combined pollution, Appl. Catal. B 258 (2019) 118062, https://doi.org/10.1016/j.apcatb.2019.118062.
[23] M. Bellardita, V. Loddo, L. Palmisano, Formation of high added value chemicals by photocatalytic treatment of biomass, Mini-Rev. Org. Chem. 17 (2020) 884–901, https://doi.org/10.2174/1570193X17666200131112856.
[24] C.M. Pecoraro, L. Mino, E. Kozyr, L. Palmisano, F. di Franco, V. Loddo, M. Santamaria, M. Bellardita, Pt–TiO₂ catalysts for glycerol photoreforming: comparison of anatase, brookite and rutile polymorphs, Chem. Commun. 60 (2024) 3782–3785, https://doi.org/10.1039/D4CC00353E.
[25] M.O. Segovia-Guzmán, M. Román-Aguirre, J.Y. Verde-Gomez, V.H. Collins-Martínez, G. Zaragoza-Galán, V.H. Ramos-Sánchez, Green Cu₂O/TiO₂ heterojunction for glycerol photoreforming, Catal. Today 349 (2020) 88–97, https://doi.org/10.1016/j.cattod.2018.05.031.
[26] M. Russo, G. Iervolino, V. Vaiano, W-doped ZnO photocatalyst for the degradation of glyphosate in aqueous solution, Catalysts 11 (2) (2021) 234, https://doi.org/10.3390/catal11020234.
[27] E.N. Musa, S. Kaur, T.C. Gallagher, T.M. Anthony, W.F. Stickle, L. Arnadottir, K. C. Stylianou, Two birds, one stone: coupling hydrogen production with herbicide degradation over metal–organic framework-derived titanium dioxide, ACS Catal. 13 (2023) 3710–3722, https://doi.org/10.1021/acscatal.3c00265.
[28] S. Chen, Y. Liu, Study on the photocatalytic degradation of glyphosate by TiO₂ photocatalyst, Chemosphere 67 (5) (2007) 1010–1017, https://doi.org/10.1016/j.chemosphere.2006.10.054.
[29] F.J. Silerio-Vázquez, M. García-Roig, L.A. González-Burciaga, C.M. Nunez-Nunez, J.B. Proal-Nájera, Glyphosate photocatalytic degradation: exploring trends, innovations and research gaps, J. Water Process. Eng. 62 (2024) 105948, https://doi.org/10.1016/j.jwpe.2024.105948.
[30] G.J. Bamiduro, C.M. Dollar, S. Abaddi, N. Ensinger, E.M. Zahran, Rapid photocatalytic mineralization of glyphosate by Pd@BiVO₄/BiOBr nanosheets: mechanistic studies and degradation pathways, Catal. Commun. 174 (2023) 106599, https://doi.org/10.1016/j.catcom.2023.106599.
[31] A. Patsoura, D.I. Kondarides, X.E. Verykios, Enhancement of photoinduced hydrogen production from irradiated Pt/TiO₂ suspensions with simultaneous degradation of azo-dyes, Appl. Catal. B 64 (2006) 171–179, https://doi.org/10.1016/j.apcatb.2005.11.015.
[32] A. Di Paola, G. Cufalo, M. Addamo, M. Bellardita, R. Campostrini, M. Ischia, R. Ceccato, L. Palmisano, Photocatalytic activity of nanocrystalline TiO₂ (brookite, rutile and brookite-based) powders prepared by thermohydrolysis of TiCl₄ in aqueous chloride solutions, Colloids Surf. A Physicochem. Eng. Asp. 317 (2008) 366–376, https://doi.org/10.1016/j.colsurfa.2007.11.005.
[33] D.R. Eddy, M.D. Permana, L.K. Sakti, G.A.N. Sheha, H. Solihudin, S. Hidayat, T. Takei, N. Kumada, I. Rahayu, Heterophase polymorph of TiO₂ (anatase, rutile, brookite, TiO₂(B)) for efficient photocatalyst: fabrication and activity, Nanomaterials 13 (2023) 704, https://doi.org/10.3390/nano13040704.
[34] N.S. Allen, N. Mahdjoub, V. Vishnyakov, P.J. Kelly, R.J. Kriek, The effect of crystalline phase (anatase, brookite and rutile) and size on the photocatalytic activity of calcined polymorphic titanium dioxide (TiO₂), Polym. Degrad. Stab. 150 (2018) 31–36, https://doi.org/10.1016/j.polymdegradstab.2018.02.008.
[35] Y. Li, B. Wang, S. Liu, X. Duan, Z. Hu, Synthesis and characterization of Cu₂O/TiO₂ photocatalysts for H₂ evolution from aqueous solution with different scavengers, Appl. Surf. Sci. 324 (2015) 736–744, https://doi.org/10.1016/j.apsusc.2014.11.027.
[36] J.-L. Chen, M.-M. Liu, S.-Y. Xie, L.-J. Yue, F.-L. Gong, K.-M. Chai, Y.-H. Zhang, Cu₂O-loaded TiO₂ heterojunction composites for enhanced photocatalytic H₂ production, J. Mol. Struct. 1247 (2022) 131294, https://doi.org/10.1016/j.molstruc.2021.131294.
[37] Z. Xi, C. Li, L. Zhang, M. Xing, J. Zhang, Synergistic effect of Cu₂O/TiO₂ heterostructure nanoparticle and its high H₂ evolution activity, Int. J. Hydrog. Energy 39 (2014) 6345–6353, https://doi.org/10.1016/j.ijhydene.2014.01.209.
[38] H. Xu, S. Ouyang, D. Wang, J. Ye, L. Liu, T. Kako, Porous-structured Cu₂O/TiO₂ nanojunction material toward efficient CO₂ photoreduction, Nanotechnology 25 (2014) 165402, https://doi.org/10.1088/0957-4484/25/16/165402.
[39] Y.-H. Zhang, M.-M. Liu, J.-L. Chen, K.-F. Xie, S.-M. Fang, Dendritic branching Z-scheme Cu₂O/TiO₂ heterostructure photocatalysts for boosting H₂ production, J. Phys. Chem. Solids 152 (2021) 109948, https://doi.org/10.1016/j.jpcs.2021.109948.
[40] M. Abdennouri, A. Elhalil, M. Farnane, H. Tounsadi, F.Z. Mahjoubi, R. Elmoubarki, M. Sadiq, L. Khamar, A. Galadi, M. Baâlala, M. Bensitel, Photocatalytic degradation of 2,4-D and 2,4-DP herbicides on Pt/TiO₂ nanoparticles, J. Saudi Chem. Soc. 19 (2015) 485–493, https://doi.org/10.1016/j.jscs.2015.06.007.
[41] C.R. López, M.N. Suárez Rodríguez, J.M. Doña Rodríguez, J.A. Navío Santos, D. Fernández Hevia, E. Pulido Melián, J.A. Ortega Méndez, Ó. González-Díaz, Hydrogen production using Pt-loaded TiO₂ photocatalysts, Int. J. Hydrog. Energy (2013), https://doi.org/10.1016/j.ijhydene.2013.07.006.
[42] M. Umair, A. Ruiz-Aguirre, I. Berruti, S. Malato Rodríguez, L. Palmisano, V. Loddo, M. Bellardita, Biomass derivatives photoreforming in pilot plant scale to obtain H₂ under green conditions by using ball milling Cu₂O–TiO₂ P25 photocatalysts, Chem. Eng. J. 504 (2025) 158585, https://doi.org/10.1016/j.cej.2024.158585.
[43] U.G.E.N. Balachandran, N.G. Eror, Raman spectra of titanium dioxide, J. Solid. State Chem. 42 (1982) 276–282, https://doi.org/10.1016/0022-4596(82)90006-8.
[44] J.C. Parker, R.W. Siegel, Calibration of the Raman spectrum to the oxygen stoichiometry of nanophase TiO₂, Appl. Phys. Lett. 57 (1990) 943, https://doi.org/10.1063/1.104274.
[45] J. Liqiang, Y. Qu, B. Wang, S. Li, B. Jiang, L. Yang, W. Fu, H. Fu, J. Sun, Review of photoluminescence performance of nano-sized semiconductor materials and its relationships with photocatalytic activity, Sol. Energy Mater. Sol. Cells 90 (2006) 1773–1787, https://doi.org/10.1016/j.solmat.2005.11.007.
[46] P. Krishnan, M. Liu, P. Itty, et al., Characterization of photocatalytic TiO₂ powder under varied environments using near ambient pressure X-ray photoelectron spectroscopy, Sci. Rep. 7 (2017) 43298, https://doi.org/10.1038/srep43298.
[47] Y. Wang, S. Liu, C. Pei, Q. Fu, Z.-J. Zhao, R. Mu, J. Gong, Modulating the surface defects of titanium oxides and consequent reactivity of Pt catalysts, Chem. Sci. 10 (2019) 10531–10536, https://doi.org/10.1039/C9SC03119G.
[48] B. Bharti, S. Kumar, H.N. Lee, et al., Formation of oxygen vacancies and Ti^{3+} state in TiO₂ thin film and enhanced optical properties by air plasma treatment, Sci. Rep. 6 (2016) 32355, https://doi.org/10.1038/srep32355.
[49] B. de la Fuente, J. Bomnuter, M. del Moro, L. Smeesters, V. Cristaudo, T. Breugelmans, V. Meynen, P. Cool, A. Hubin, T. Hauffman, On the combination of ultraviolet photoelectron spectroscopy with optical absorption studies to investigate Cu₂O||TiO₂ direct Z-scheme junctions with different Cu₂O loading, Appl. Surf. Sci. 657 (2024) 159796, https://doi.org/10.1016/j.apsusc.2024.159796.
[50] F. Plascencia-Hernández, E. Albiter, G.M. Nawfal, C. Colbeau-Justin, H. Remita, H. Pfeiffer, M.A. Valenzuela, Unraveling the effect of low Cu₂O loading on P25 TiO₂ and its self-reduction during methanol photoreforming, Inorg. Chem. Commun. 158 (1) (2023) 111541, https://doi.org/10.1016/j.inoche.2023.111541.
[51] K. Roy, C.S. Gopinath, UV photoelectron spectroscopy at near ambient pressures: mapping valence band electronic structure changes from Cu to CuO, Anal. Chem. 86 (2014) 3683–3687, https://doi.org/10.1021/ac4041026.
[52] Y. Wang, Y. Lü, W. Zhan, Z. Xie, Q. Kuang, L. Zheng, Synthesis of porous Cu₂O/CuO cages using Cu-based metal–organic frameworks as templates and their gas-sensing properties, J. Mater. Chem. A 3 (2015) 12796–12803, https://doi.org/10.1039/C5TA01108F.
[53] R.H. Adnan, A.A. Jalil, Gold photocatalysis in sustainable hydrogen peroxide generation, Mater. Today Chem. 27 (2023) 101322, https://doi.org/10.1016/j.mtchem.2022.101322.
[54] M. Bellardita, H.A. El Nazer, V. Loddo, F. Parrino, A.M. Venezia, L. Palmisano, Photoactivity under visible light of metal loaded TiO₂ catalysts prepared by low frequency ultrasound treatment, Catal. Today 284 (2017) 92–99, https://doi.org/10.1016/j.cattod.2016.11.026.
[55] H.B. Michaelson, The work function of the elements and its periodicity, J. Appl. Phys. 48 (1977) 4729–4733, https://doi.org/10.1063/1.323539.
[56] A. Di Paola, M. Bellardita, R. Ceccato, L. Palmisano, F. Parrino, Highly active photocatalytic TiO₂ powders obtained by thermohydrolysis of TiCl₄ in water, J. Phys. Chem. C. 113 (2009) 15166–15174, https://doi.org/10.1021/jp904673e.
[57] J. Buckeridge, K.T. Butler, C.R.A. Catlow, A.J. Logsdail, D.O. Scanlon, S.A. Shevlin, S.M. Woodley, A.A. Sokol, A. Walsh, Polymorph engineering of TiO₂: demonstrating how absolute reference potentials are determined by local coordination, Chem. Mater. 27 (2015) 3844–3851, https://doi.org/10.1021/acs.chemmater.5b00230.
[58] M. Bellardita, V. Augugliaro, V. Loddo, B. Megna, G. Palmisano, L. Palmisano, M. A. Puma, Selective oxidation of phenol and benzoic acid in water via home-prepared TiO₂ photocatalysts: distribution of hydroxylation products, Appl. Catal. A Gen. 441 (2012) 79–89, https://doi.org/10.1016/j.apcata.2012.07.019.
[59] Q.Y. Tang, M.J. Yang, S.Y. Yang, Y.H. Xu, Enhanced photocatalytic degradation of glyphosate over 2D CoS/BiOBr heterojunctions under visible light irradiation, J. Hazard. Mater. 407 (2021) 124798, https://doi.org/10.1016/j.jhazmat.2020.124798.
[60] J. Chrobak, J. Ilowska, A. Chrobok, Formaldehyde-free resins for the wood-based panel industry: alternatives to formaldehyde and novel hardeners, Molecules 27 (2022) 4862, https://doi.org/10.3390/molecules27154862.
[61] P. Solt, J. Konnerth, W. Gindl-Altmutter, W. Kantner, J. Moser, R. Mitter, H.W. G. van Herwijnen, Technological performance of formaldehyde-free adhesive alternatives for particleboard industry, Int. J. Adhes. Adhes. 94 (2019) 99–131, https://doi.org/10.1016/j.ijadhadh.2019.04.007.
[62] A. Álvarez, A. Bansode, A. Urakawa, A.V. Bavykina, T.A. Wezendonk, M. Makkee, J. Gascon, F. Kapteijn, Challenges in the greener production of formates/formic acid, methanol, and DME by heterogeneously catalyzed CO_2 hydrogenation processes, Chem. Rev. 117 (2017) 9804–9838, https://doi.org/10.1021/acs.chemrev.7b00159.
[63] D.R. Jarois, L.E. Schimmelpfennig, S.H. Gellman, A new mechanism for formation of glycine from glyoxylic acid: the Aza-Cannizzaro reaction, Chem. Eur. J. 30 (2024) e202403202, https://doi.org/10.1002/chem.202403202.
[64] P. D'Arrigo, L.A.M. Rossato, A. Strini, S. Serra, From waste to value: recent insights into producing vanillin from lignin, Molecules 29 (2024) 442, https://doi.org/10.3390/molecules29020442.
[65] L. Liu, A. He, X. Li, Synthesis of allantoin catalyzed by SO_4^{2-}/La_2O_3-SiO_2-ZrO_2, Asian J. Chem. 24 (2012) 2298.
[66] S.M. Ali, A.I. Alwared, Photocatalytic detoxification of glyphosate herbicide in water using visible-light active g-C_3N_4/Fe_3O_4/$CuWO_4$/CuO nanocomposites, S. Afr. J. Chem. Eng. 56 (2026) 100865, https://doi.org/10.1016/j.sajce.2026.100865.